Tuning Aggregation of Poly-(3-hexylthiophene) within Nanoparticles

Gavvalapalli Nagarjuna,[†] Mina Baghgar,[‡] Joelle A. Labastide,[†] Dana D. Algaier,[†] Michael D. Barnes,[†,‡,*] and Dhandapani Venkataraman[†,*]

[†]Department of Chemistry and [‡]Department of Physics, University of Massachusetts Amherst, 710 North Pleasant Street, Amherst, Massachusetts 01003, United States

ABSTRACT Nanoparticles derived from π-conjugated polymers have gained widespread attention as active layer materials in various organic electronics applications. The optoelectronic, charge transfer, and charge transport properties of π-conjugated polymers are intimately connected to the polymer aggregate structure. Herein we show that the internal aggregate structure of regioregular poly(3-hexylthiophene) (P3HT) within polymer nanoparticles can be tuned by solvent composition during nanoparticle fabrication through the miniemulsion process. Using absorption spectra and single-NP photoluminescence decay properties, we show that a solvent mixture consisting of a low boiling good solvent and a high boiling marginal solvent results in polymer aggregate structure with a higher degree of uniformity and structural order. We find that the impact of solvent on the nature of P3HT aggregation within nanoparticles is different from what has been reported in thin films.

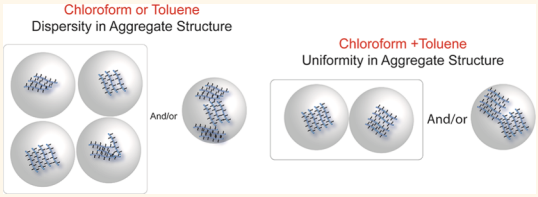

KEYWORDS: nanoparticles · poly(3-hexylthiophene) · aggregates · internal structure · photophysics · and miniemulsion

Nanoparticles derived from conjugated polymers are currently the subject of intense research effort for potential applications in sensors,[1−4] optical imaging,[5−11] and as building blocks for active layer structures in optoelectronic devices.[12−39] Recently, we reported a strategy for controlling the morphology of active layers in organic photovoltaic cells using nanoparticles derived from conjugated polymers.[40,41] The central advantage of a nanoparticle-based approach is that domains of electron- and hole-transporting polymers can be preformed with tunable size and internal aggregate structure which can then self-assemble into well-defined crystal packing structures forming the active layer of polymer-based photovoltaic cells. Since both charge-separation and charge-transport processes are intimately connected with the polymer aggregate structure within the nanoparticle,[41] it is vital to control the polymer aggregation within the nanoparticle and to understand the impact of the internal structure of the nanoparticle on the optoelectronic properties.[30,42,43] In this paper, we show that the aggregate structure within the polymer nanoparticles can be tuned by solvent composition during nanoparticle fabrication through the miniemulsion process as evidenced by differences in aggregate absorption spectra and single-NP photoluminescence decay properties.

We chose regioregular poly(3-hexylthiophene) (P3HT) for our investigation because it has been one of the most studied conjugated polymers and thus can serve as an excellent benchmark for us to compare and unravel the impacts of confinement on the optoelectronic properties.[44] P3HT is well-known for its propensity to aggregate into crystalline domains in thin films, and both charge-separation and charge transport processes are known to depend on the nature of aggregation of the polymer in thin films.[45−56] It is known that P3HT thin films obtained from chloroform (a "good" solvent for P3HT) show poor intrachain order and crystallinity compared to films cast from marginal solvents for P3HT such as toluene that show enhanced intrachain order with longer conjugation lengths and higher crystalline quality.[57−59] These results point to both solvent quality and vapor pressure as playing key roles in thin-film aggregation.

The solvent effects are also prominent in the solution-phase assembly of two-dimensional nanofibers or nanowires of P3HT. As shown recently by Moule, Spano and co-workers, local aggregate structure with

* Address correspondence to dv@chem.umass.edu, mdb@chem.umass.edu.

Received for review August 31, 2012 and accepted November 25, 2012.

Published online November 25, 2012
10.1021/nn305207b

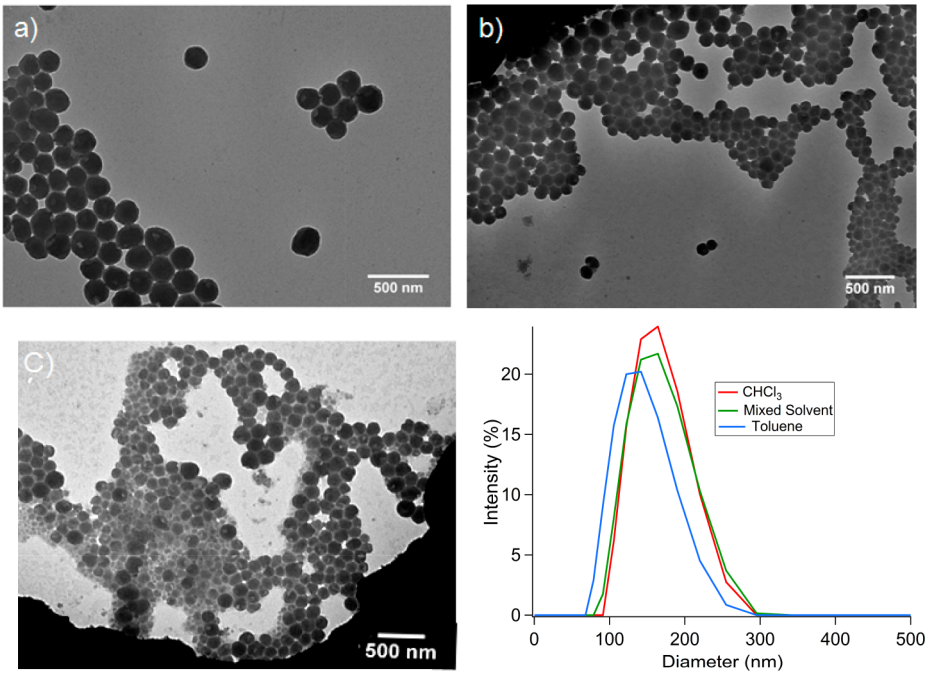

Figure 1. Representative TEM images of the P3HT nanoparticles synthesized from (a) chloroform, (b) toluene/chloroform (1:4 v/v), (c) toluene, and (d) intensity particle size distribution of P3HT nanoparticles obtained from DLS.

varying degrees of intra- and interchain order is highly sensitive to solvent and crystallization kinetics.[57,59] However, a key difference between 2-D nanofibers and nanoparticles is the fact that in nanofiber self-assembly the polymer chains pack in a well-defined way, with formation of lamellar sheets assembled by $\pi-\pi$ interactions. In nanoparticles—in particular, where the nanoparticle diameter is comparable to the contour length of the polymer—the chain packing can be frustrated both kinetically (by trapping in metastable configurations) as well as spatially where nanoparticle surface curvature might be important. In our recent work on photoluminescence properties of individual P3HT nanoparticles, we observed significant differences in both short- and long-time photoluminescence properties with varying nanoparticle size, an effect that was interpreted as a result of size-dependent internal (aggregate) structure.[41] In this paper, we show from a combination of ensemble absorption and single-particle photoluminescence studies how the internal chain-packing structure of P3HT nanoparticles can be tuned through solvent manipulation.

RESULTS AND DISCUSSION

Stable P3HT nanoparticles were synthesized through a miniemulsion process by the injection of a P3HT (22 kDa MW, Đ = 2.13; regioregularity, 90%−93%) solution in an organic solvent (oil phase) into an aqueous surfactant solution, followed by ultrasonication, and finally removal of the organic solvent by heating.[60] We used three different solvents to fabricate P3HT nanoparticles: chloroform, toluene, and a mixture of toluene and chloroform (1:4 v/v) as the "oil" phase.

TABLE 1. Size, Peak Positions of 0−0 and 0−1 Transitions from UV/vis Absorption, and A_{0-0}/A_{0-1} Intensity of P3HT Nanoparticles Synthesized from Different Solvent Composition[a]

solvent	*Z*, nm[b] (%PDI)	λ_{A0-0} (nm)	λ_{A0-1} (nm)	A_{0-0}/A_{0-1}[c]
$CHCl_3$	142 (26)	561	610	0.71 ± 0.05
toluene/$CHCl_3$[d]	135 (33)	561	608	0.68 ± 0.03
toluene	124 (27)	559	606	0.66 ± 0.05

[a] Samples prepared from 1 mM SDS and 0.5 wt % P3HT. [b] Mean of the *Z*-average derived from intensity peak statistics and percent polydispersity from several trials. [c] Mean of several trials and the error is the standard deviation. [d] Mixture of toluene and chloroform in 1:4 (v/v) ratio.

We probed the impact of oil phase composition on nanoparticle size by synthesizing NP families from different solvents using 0.5 wt % solution of P3HT and 1 mM sodium dodecylsulfate (SDS, surfactant) concentration. Size and size-dispersity of the nanoparticles were determined using dynamic light scattering (DLS) (see Supporting Information). All samples exhibited monomodal distributions in DLS. Transmission electron microscopy (TEM) images of P3HT nanoparticles synthesized from different organic solvents using 0.5 wt % P3HT solution and 1 mM SDS are shown in Figure 1a−c. The particle size and size distribution in TEM is consistent with the DLS data. Table 1 shows the average diameter (*Z*) along with the average percent polydispersity, which is representative of the particle size distribution width, for six different nanoparticle batches synthesized for each choice of solvent

composition (see Supporting Information, Tables S1−S3 for all the data points). The P3HT nanoparticles made from chloroform were consistently larger than the particles obtained from toluene. The size of nanoparticles made from a mixture of toluene and chloroform (1:4 v/v) is in between the particle sizes obtained from chloroform and from toluene. To see if the size differences arose from inconsistencies in weighing small amounts of P3HT (~5 mg), a 0.5 wt % P3HT solution in chloroform was prepared and was equally distributed into three preweighed vials, and then the chloroform was evaporated. Vials were kept under reduced pressure over 3 h and were weighed again to determine the amount of P3HT transferred. Within experimental error, the amount of P3HT transferred into each vial was the same and was consistent with the amount of P3HT dissolved in the volume of chloroform transferred. The solvent was then added to each vial to generate 0.5 wt % P3HT solution in chloroform, toluene, and the chloroform/toluene mixture. The sizes of the nanoparticles were determined using DLS and are 122, 110, and 73 nm, respectively, reaffirming our observations. The nanoparticle dispersions have a zeta potential of about −60 mV, and UV-absorption spectra of the dispersions recorded over a period of a month is identical to that of the fresh samples, indicating the long-term stability of these dispersions.

Figure 2 (top) shows the absorption spectra (normalized to the absorbance of the 0−2 vibronic transition) for an aqueous suspension of nanoparticles formed from 0.5 wt % P3HT in chloroform, toluene, and mixed solvent. The aggregate region of the absorption spectra is similar to that seen in P3HT thin films and nanofibers, with vibronic peaks at 518, 560, and 610 nm, assigned as the A_{0-2}, A_{0-1}, and A_{0-0} peaks, respectively (subscripts denote the number of vibrational quanta coupled to electronic transitions).[41,57,61] The measured absorption spectra are composed of two parts: a high-energy region that is attributed to unaggregated (amorphous) P3HT chains, and a low energy region that carries the vibronic structure of aggregate P3HT within NPs. Given the fact that P3HT chains cannot be dissolved in aqueous solution and are encapsulated during droplet formation in aqueous surfactant solution indicates that the amorphous absorption is due to unaggregated chains *within* the nanoparticles, not from free P3HT in the suspension. It is interesting to note that decreasing solvent quality does not affect the contribution of the amorphous component to the absorption spectra, but does appear to affect the intensity of 0−0 and 0−1 vibronic peaks (relative to 0−2 absorption).

From a decomposition of the absorption spectra into aggregate and amorphous components (by subtraction of an appropriately scaled amorphous P3HT absorption spectrum of a dilute P3HT solution in chloroform from the measured spectrum), we estimated the

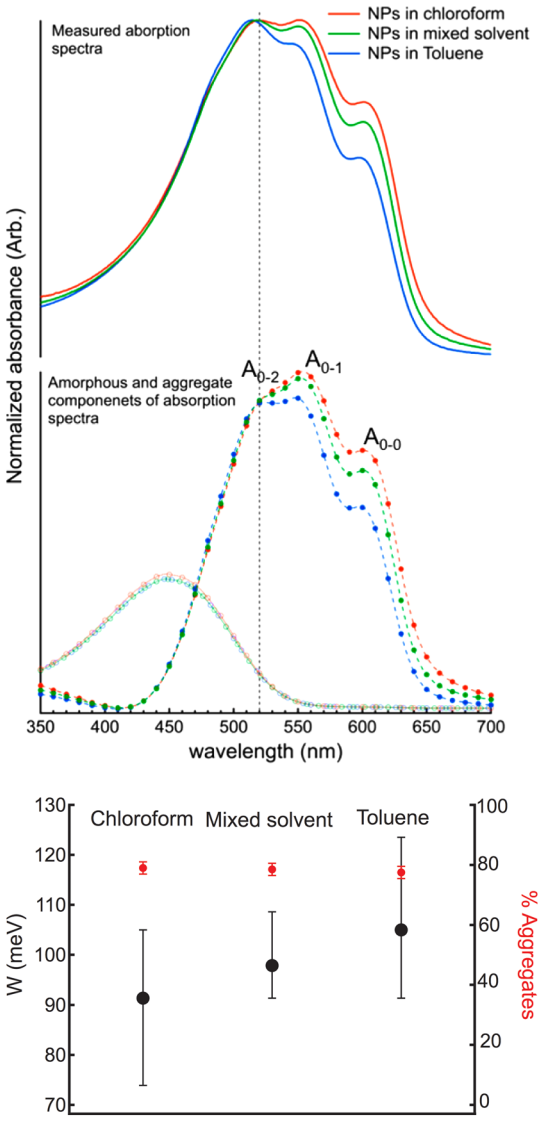

Figure 2. (a, top) Normalized absorption spectra of P3HT nanoparticles assembled from solution in chloroform (red), toluene (blue), and 4:1 mixture of chloroform and toluene (green); (a, bottom) open-circled line and close-circled line show the amorphous absorption and aggregate absorption, respectively, in each NPs spectra. Vertical dashed-line indicates the A_{0-2} peak position (520 nm) and separates the solvent quality-dependent part of the absorption spectra from the region that is fairly affected by solvent. (b) Free exciton bandwidth (black) and crystal fraction (red) for different solvent compositions.

relative amounts of amorphous and crystalline material for each family of P3HT NPs. In P3HT thin-films and nanofibers, the contribution of the aggregate component to the total absorption increases as the amorphous component decreases, and both change with decreasing solvent quality.[57,59] In contrast, the contribution of the amorphous and aggregate structural components of the nanoparticle appear to be completely insensitive to the choice of oil phase, but the aggregate contribution to the *spectrum* tends to decrease with decreasing solvent quality. This indicates the change in the quantum yield of the aggregate

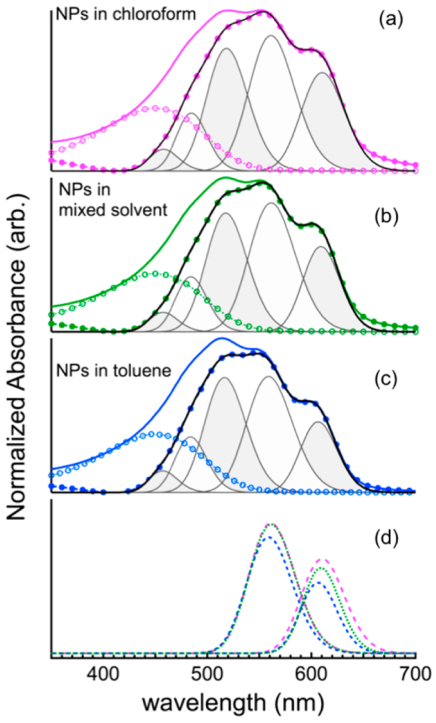

Figure 3. Experimental absorption spectra normalized to 0−2 absorption strength for NPs formed from 15 kDa P3HT solution in (a) chloroform (solid red line), (b) 4:1 mixture of chloroform and toluene (solid green line), and (c) toluene (solid blue line). Each absorption spectrum was decomposed into a scaled unaggregated P3HT (in $CHCl_3$) component (open circles), and aggregate spectrum (closed circles) modeled as a progression of five Gaussian functions with fwhm, peak position, and peak extinction coefficient as adjustable parameters. (d) The first two Gaussian components corresponding to 0−0 and 0−1 transitions in the absorbance spectrum of each NPs family presented in panels a−c.

species due to the solvent-dependence of the crystal structure. Since NPs from different solvents are made with the same amount of polymer, we can infer that the percentage of unaggregated chains within NPs does not depend on solvent quality. Thus the solvent quality affects the aggregate absorption through changing the crystalline order and not the actual amount of the aggregated chains.

There have been several studies correlating the relative intensities of vibronic features in the absorption spectra of P3HT thin films with P3HT aggregate structure.[47,49,53,55,62−66] In the *H*/*J* aggregate model developed by Spano, information on both dominant coupling types, *H*-type (face-to-face), or *J*-type (end-to-end), and coupling magnitude (exciton bandwidth, *W*) is encoded in the intensity ratio of the origin (0−0) and first vibronic satellite (0−1) transitions by the relation[67]

$$\frac{A_{0-0}}{A_{0-1}} = \left(\frac{1 - 0.24W/\omega_o}{1 + 0.073W/\omega_o}\right)^2 \quad (1)$$

where *W* is the exciton bandwidth ($W = 4\,|J_0|$, where J_0 is the exciton coupling matrix element); and ω_0 is the vibrational energy of the symmetric vinyl stretch

TABLE 2. Fit Parameters of the Gaussian Components Assigned to the Different Vibronic Components of the P3HT NP Absorption Spectra[a]

oil phase	A_{0-0}/A_{0-2}	σ_0 (meV)	A_{0-1}/A_{0-2}	σ_1 (meV)	Δ_{01} (meV)	A_{0-0}/A_{0-1}
$CHCl_3$	0.62	$0.91\omega_0$	0.84	$1.14\omega_0$	178	0.73
$CHCl_3$/toluene	0.55	$0.78\omega_0$	0.84	$1.14\omega_0$	173	0.65
toluene	0.46	$0.78\omega_0$	0.75	$1.14\omega_0$	174	0.61

[a] σ_n is the fwhm of the 0-n vibronic transition, Δ_{01} is the energy spacing between the first two (0−0, and 0−1) vibronic transitions. These values are typically smallar than the "accepted" value of ω_0 (180 meV). Note also the increase in line width for the higher sidebands.

(taken here to be 0.178 eV). The dominant coupling type can be readily identified from measurement of the 0−0 and 0−1 absorption strengths,[46,52,53,55,68] where the primary conditions for validity are that (1) only nearest-neighbors coupling is considered and (2) only one aggregate type (*H* or *J*) contributes to the electronic absorption. *H*-type aggregation typically dominates in a system with a high degree of torsional disorder (shorter conjugation length), while *J*-type coupling is typically seen (for example, in nanofibers) in systems with a high degree of planarity of thiophene rings.

Figure 3 shows the aggregate spectrum for each of the three NP families (from chloroform, toluene, and 1:4 mixture of toluene and chloroform) modeled as a single vibronic progression of five peaks in which intensity (related to Huang−Rhys factor), peak position, and transition line width were treated as adjustable parameters. As indicated in Table 1, we found that the A_{0-0}/A_{0-1} ratio was less than 1 for all three oil phases, suggestive of a weakly coupled *H*-aggregate ($J_0 \approx +20$ meV). The calculated free-exciton bandwidth *W* presented in Figure 2b shows that the average value of *W* increases with decreasing solvent quality, however the distribution of *W* values is large for both chloroform and toluene formed nanoparticles, and narrow for the mixture. It is noteworthy that these values of *W* lie somewhat in between values seen in P3HT thin-films, although the trend with solvent quality is opposite to that seen in thin films.[59]

In modeling the aggregate absorption spectra we observed two subtle and interesting features: (1) for all the NP samples a significant anharmonicity of about 15−20 meV must be introduced to fit the observed absorption spectra, and (2) the linewidths for the higher aggregate sidebands increase substantially with respect to the 0−0 origin. These features indicate that the P3HT nanoparticle absorption spectra are *not* a simple composition of amorphous and single *H*- or *J*-aggregate species. This issue will be addressed in more detail elsewhere. Further analysis of the aggregate absorption spectra indicated (see Figure 3d and Table 2) that as the (oil-phase) solvent quality decreases, the electronic origin is blue-shifted by about 2 nm (6 meV) for the mixed solvent and 4 nm (11 meV)

for toluene compared to NPs obtained from chloroform, which is suggestive of an increase in torsional disorder and thus shorter conjugation length. This observation of blue-shifted electronic origin along with slightly higher value for exciton bandwidth (*W*), and the reduction in fwhm by ~10% are suggestive of a higher degree of structural order (reduced inhomogeneous broadening) in the nanoparticle samples from mixed solvent and toluene (Table 2).

We obtained further insight into the influence of the polymer solvent on nanoparticle aggregate structure within the nanoparticle through time-resolved photoluminescence (PL) measurements on single nanoparticles. For detailed information on the short-time decay dynamics, PL measurements were done using time-tagged-time-resolved (TTTR) single photon counting with 16 ps resolution over a 50 ns time window. We used a PicoQuant pulsed diode laser head operating at 440 nm wavelength and 50 ps pulse width, in a weakly focused epi-illumination geometry (spot size $\approx$ 20 μm diameter). The input intensity was approximately 1 kW/cm^2, with an instrument response fwhm of 180 ps. The photoluminescence decay dynamics from the different P3HT nanoparticle families studied here are approximately a double exponential at early times (less than 5 ns). The first decay component ($t \approx$ 150 ps) dominated the photoluminescence, accounting for more than 94% of the total amplitude, while the second decay process ($t \approx$ 1.5 ns) typically accounted for <6% of total amplitude.

Figure 4 shows the contribution (amplitude) of each decay component as a function of their respective time constants for single nanoparticles made from chloroform, toluene, and chloroform/toluene. We have indicated the PL-count rate with color-saturation to illustrate the correlation between fluorescence intensity and both the amplitude and value of the fluorescence lifetime components—particularly that of the prompt component. In extended nanofibers of P3HT dispersion in the amplitude/lifetime correlations is indicative of heterogeneity in the local environments experienced by polymer chains within an aggregate. In the nanoparticle, packing defects that are likely to cause site heterogeneity are hypothesized to be a result of stress due to the curved confinement, and are therefore sensitive to nanoparticle size. Atomic force microscopy (AFM) correlated photoluminescence measurements (to be published elsewhere) revealed that, under constant laser power, nanoparticles of similar sizes gave similar PL count rates. Therefore the PL intensity value distribution reflects approximately the size distribution within each sample. Curiously, the size dependence seems to be much more important in the nanoparticles made from the pure solvents than it is in the mixed solvent-formed particles. The convergence of the amplitude/lifetime correlation distributions in the chloroform/toluene particles is likely due to the

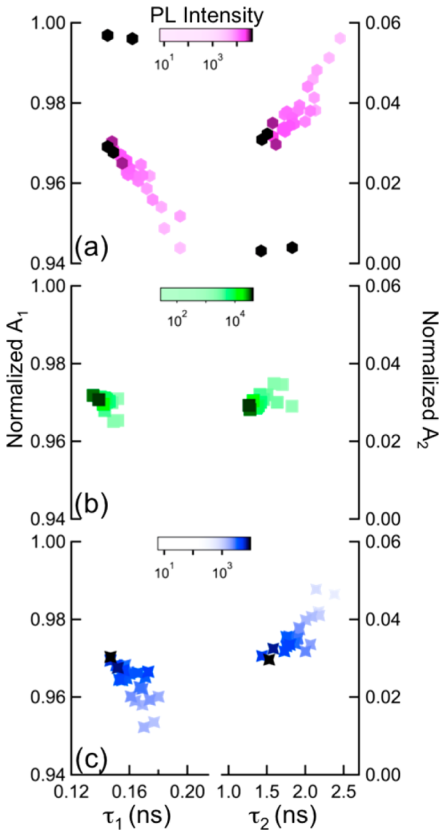

Figure 4. Correlation plot of normalized amplitude *vs* lifetime of the prompt component to the total PL decay of nanoparticles made from 5 mg/mL solutions of P3HT in (a) chloroform (136 nm), (b) 4:1 chloroform/toluene (116 nm), and (c) toluene (98 nm). The color saturation shows the PL count rate for individual NP measurement within a particular NP sample.

degree of uniformity in the internal environment: a result of the kinetically favorable crystallization process afforded by the properties of the mixed solvent.

The absorption spectrum of P3HT nanostructures and thin films is a widely employed tool for determining crystalline fraction and aggregate type. However, the linewidths of the vibronic transitions (origin and sidebands) carry important information on the degree of inhomogeneity in the aggregate structure, and are often overlooked during analysis. The lifetime distributions from time-resolved fluorescence measurements also indicated differences in the nature of the aggregates within the nanoparticles. The large inhomogeneous broadening seen in the origin transition for the chloroform nanoparticles, as well as the divergence of the amplitude/lifetime correlation distribution for these particles, reveal that NPs from chloroform have the largest degree of internal structural *disorder*. On the basis of this observation and from the analysis of the aggregate absorption spectra (particularly the fwhm of different vibronic components), we conclude that there is a higher degree of structural uniformity in the polymer aggregates for nanoparticles synthesized from mixed solvents.

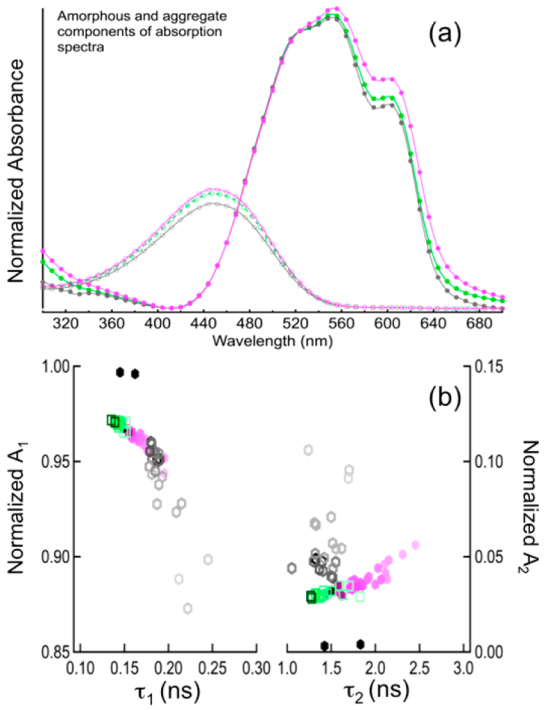

Figure 5. (a) Aggregate and amorphous components of the absorption spectra of P3HT nanoparticles assembled from chloroform at 80 °C (pink) and 60 °C (gray), and mixed solvent at 80 °C (green). (b) Amplitude/lifetime correlation plot for nanoparticles in panel a.

The absorption and photoluminescence data collectively indicate that the impact of solvent on P3HT aggregation within the nanoparticle is different from what has been observed in thin films. We find that order in the polymer aggregate structure is superior with a higher degree of uniformity if the oil phase contains a mixture of a marginal solvent and a good solvent for the conjugated polymer.

Figure 5a shows the aggregate and amorphous components of the absorption spectra from nanoparticle families made from chloroform that was evaporated at 80 °C (magenta) and 60 °C (gray) and the mixed solvent (green) evaporated at 80 °C. Upon inspection of the absorption spectra for this set, it would appear that by decreasing the evaporation temperature in the single solvent nanoparticles, we can reproduce the characteristics seen in the mixed solvent particles. However, the amplitude/lifetime correlation plot shown in Figure 5b of the same three particle families reveals different internal structural characteristics for low-temperature chloroform and mixed solvent particles. While the high temperature chloroform distribution (magenta) of short-time decay components underlies both the low temperature chloroform (gray) and mixed solvent (green) distributions, they represent different and nonoverlapping subsets. This indicates that there is a notable difference in the efficiency of the radiative decay processes in the aggregate species, and that the effect of the mixed solvent on the crystallization

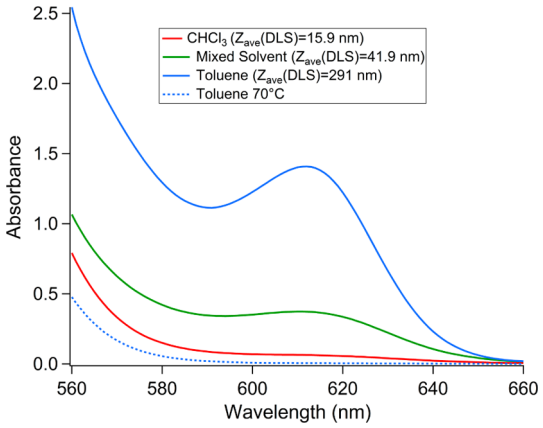

Figure 6. (a) UV−vis absorption spectra of P3HT in various solvents. The presence of a peak around 610 nm indicates the presence of P3HT aggregates. The sizes of the P3HT aggregates measured by dynamic light scattering of 0.5 wt % P3HT solution in different solvents are shown in the figure key. For clarity absorption spectra is shown between 560 and 660 nm.

equilibrium is not simply due to slow evaporation caused by toluene's higher boiling point.

In thin films, which are typically cast at room temperature, there are no spatial restrictions on the polymer conformation or on the aggregation process. Therefore, the solubility of the polymer in the chosen solvent at room temperature and the boiling point of the solvent play key roles in the final aggregate structure. The formation of nanoparticles through a miniemulsion process involves formation of micrometer-sized solvent droplets upon ultrasonication (see Figure S7 in the Supporting Information) followed by the evaporation of the solvent at elevated temperatures. In the first stage, based on absorption spectra and DLS, the polymer is substantially dissolved in chloroform and in chloroform/toluene (Figure 6); the polymer is aggregated in toluene. The ultrasonication process in the miniemulsion process can induce polymer aggregation but this effect is mostly negated by heating.[68] At 80 °C, P3HT is soluble in chloroform and in toluene and there are no signatures of aggregation in the absorption spectra at this temperature in either of the solvents. Upon heating at 80 °C, the solvent evaporates and the droplets shrink in size. During this process, the effective concentration of the polymer within the droplet increases. If the oil phase is chloroform, then the color of the emulsion abruptly changes from milky orange to clear purple, which is the color of a P3HT thin film. Since chloroform is a good solvent for P3HT (solubility $\approx$ 14 mg/mL),[69] the polymer chain are expected to have a higher degree of chain mobility and conformational freedom. However, at 80 °C, the rapid evaporation of chloroform triggers fast polymer aggregation. Since most if not all the chloroform is removed rapidly at 80 °C, the polymer aggregates cannot be solvent annealed and therefore remain kinetically trapped leading to a higher degree of

dispersity in polymer aggregates. If the oil phase is toluene, then as the concentration of the polymer within the droplet increases, since toluene is a marginal solvent for P3HT (solubility ≈ 0.7 mg/mL), the polymer will start to aggregate before most of the solvent is removed. Moreover, at 80 °C, the evaporation rate of toluene is much slower compared to that of chloroform. Therefore, the aggregates can anneal as the solvent is evaporating. This annealing process may contribute to a tighter packing of the polymer chains, leading to smaller particle size compared to that of chloroform. In the mixed solvent system, the solubility of the polymer is lowered but the presence of good solvent enhances the chain mobility thereby allowing the aggregates to solvent-anneal resulting in a higher degree of uniformity and structural order.

CONCLUSION

In summary, we have shown that the solvent (oil phase) is a powerful knob to tune the aggregation of P3HT within the nanoparticles. We find that using a solvent mixture of a good solvent and a marginal solvent provides structurally ordered P3HT aggregates within nanoparticles. We also find that the impact of solvent on the nature of P3HT aggregation within nanoparticles is different from the impact seen in thin films. Detailed investigations of the absorbance and photoluminescence spectrum of the nanoparticles are currently underway and will be reported in due course.

METHODS

Materials. P3HT (4002-EE, M_w = 52.3 kDa, Đ = 2.15 and regioregularity = 90−93%) was purchased from commercial vendors. Sodium dodecyl sulfate (SDS) was purchased from Sigma Aldrich. Solvents were purchased from Fisher (optima grade). Purified water (resistance 10 Mohms) was used for the synthesis of nanoparticles.

Synthesis of P3HT Nanoparticles. In a typical synthesis of P3HT nanoparticles, P3HT of a desired concentration was dissolved in a desired organic solvent. This solution was slightly warmed to ensure the complete solubility of P3HT. P3HT of 0.5 mg/mL concentration is bright orange in color for all three organic solvents used in this study. P3HT of 5 mg/mL concentration is bright orange color in chloroform and chloroform/toluene mixtures, whereas in toluene the solution is dark red. SDS solutions of desired concentration were prepared using purified water, then warmed and bath sonicated to ensure complete solubility. During the preparation of SDS solutions, caution was taken to prevent foaming by not shaking the solution vigorously to solubilize SDS. Also, during the synthesis of nanoparticles, the solution was transferred slowly *via* syringe. SDS solutions were filtered through syringe filters before use in the synthesis of nanoparticles. A 2.5 mL aliquot of SDS solution was taken in a 20 mL vial and ~0.35 mL P3HT solution was taken in a 7 mL vial. Both solutions were sonicated for 10 s, and 0.25 mL of P3HT solution was immediately injected rapidly into the SDS solution using a 1 mL syringe fitted with a 22G11/2 needle. The resulting solution was immediately ultrasonicated for 2 min at 6 W power. During ultrasonication, the probe was submerged halfway into the solution at the same time not touching the vial throughout the ultrasonication. After ultrasonication, a magnetic stir bar was added into the emulsion and the vial was immersed into a preheated oil bath to evaporate organic solvent. The temperature of oil bath was maintained at ~85 °C and the vial was immersed into the oil bath up to the emulsion level. The vial was heated for 15 min in the case of chloroform or toluene/chloroform mixture emulsions and was heated for ~50 min in the case of toluene emulsions. The nanoparticle suspension was allowed to come to room temperature and was filtered through a PES membrane with 0.22 μm pore size and 33 mm in diameter to remove micrometer size impurities before characterization.

Conflict of Interest: The authors declare no competing financial interest.

Acknowledgment. We thank PHaSE Energy Frontier Research Center supported by the US Department of Energy, Office of Basic Energy Sciences, through Grant DE-SC0001087 (DMR 0820506) for financial support of this work.

Supporting Information Available: Methods for the preparation of nanoparticle dispersions, dynamic light scattering and electrophoretic mobility data of the nanoparticle dispersions, and absorption data for filtered and unfiltered dispersions. This material is available free of charge *via* the Internet at http://pubs.acs.org.

REFERENCES AND NOTES

1. Wu, C. F.; Bull, B.; Christensen, K.; McNeill, J. Ratiometric Single-Nanoparticle Oxygen Sensors for Biological Imaging. *Angew. Chem., Int. Ed.* **2009**, *48*, 2741–2745.
2. Pecher, J.; Mecking, S. Nanoparticles of Conjugated Polymers. *Chem. Rev.* **2010**, *110*, 6260–6279.
3. Tuncel, D.; Demir, H. V. Conjugated Polymer Nanoparticles. *Nanoscale* **2010**, *2*, 484–494.
4. Tian, Z. Y.; Yu, J. B.; Wu, C. F.; Szymanski, C.; McNeill, J. Amplified Energy Transfer in Conjugated Polymer Nanoparticle Tags and Sensors. *Nanoscale* **2010**, *2*, 1999–2011.
5. Moon, J. H.; Deans, R.; Krueger, E.; Hancock, L. F. Capture and Detection of a Quencher Labeled Oligonucleotide by Poly(phenylene ethynylene) Particles. *Chem. Commun.* **2003**, 104–105.
6. Wu, C. F.; Szymanski, C.; McNeill, J. Preparation and Encapsulation of Highly Fluorescent Conjugated Polymer Nanoparticles. *Langmuir* **2006**, *22*, 2956–2960.
7. Baier, M. C.; Huber, J.; Mecking, S. Fluorescent Conjugated Polymer Nanoparticles by Polymerization in Miniemulsion. *J. Am. Chem. Soc.* **2009**, *131*, 14267–14273.
8. Howes, P.; Green, M.; Levitt, J.; Suhling, K.; Hughes, M. Phospholipid Encapsulated Semiconducting Polymer Nanoparticles: Their Use in Cell Imaging and Protein Attachment. *J. Am. Chem. Soc.* **2010**, *132*, 3989–3996.
9. Pecher, J.; Huber, J.; Winterhalder, M.; Zumbusch, A.; Mecking, S. Tailor-Made Conjugated Polymer Nanoparticles for Multicolor and Multiphoton Cell Imaging. *Biomacromolecules* **2010**, *11*, 2776–2780.
10. Moon, J. H.; MacLean, P.; McDaniel, W.; Hancock, L. F. Conjugated Polymer Nanoparticles for Biochemical Protein Kinase Assay. *Chem. Commun.* **2007**, 4910–4912.
11. Wu, C.; Szymanski, C.; Cain, Z.; McNeill, J. Conjugated Polymer Dots for Multiphoton Fluorescence Imaging. *J. Am. Chem. Soc.* **2007**, *129*, 12904–12905.
12. Moule, A. J.; Allard, S.; Kronenberg, N. M.; Tsami, A.; Scherf, U.; Meerholz, K. Effect of Polymer Nanoparticle Formation on the Efficiency of Polythiophene Based "Bulk-Heterojunction" Solar Cells. *J. Phys. Chem. C* **2008**, *112*, 12583–12589.
13. Moule, A. J.; Meerholz, K. Morphology Control in Solution-Processed Bulk-Heterojunction Solar Cell Mixtures. *Adv. Funct. Mater.* **2009**, *19*, 3028–3036.

14. Wang, F.; Han, M. Y.; Mya, K. Y.; Wang, Y. B.; Lai, Y. H. Aggregation-Driven Growth of Size-Tunable Organic Nanoparticles Using Electronically Altered Conjugated Polymers. *J. Am. Chem. Soc.* **2005**, *127*, 10350–10355.
15. Richards, J. J.; Weigandt, K. M.; Pozzo, D. C. Aqueous Dispersions of Colloidal Poly(3-hexylthiophene) Gel Particles with High Internal Porosity. *J. Colloid Interface Sci.* **2011**, *364*, 341–350.
16. Li, X. G.; Li, J.; Huang, M. R. Facile Optimal Synthesis of Inherently Electroconductive Polythiophene Nanoparticles. *Chem.—Eur. J.* **2009**, *15*, 6446–6455.
17. Li, X. G.; Li, J.; Meng, Q. K.; Huang, M. R. Interfacial Synthesis and Widely Controllable Conductivity of Polythiophene Microparticles. *J. Phys. Chem. B* **2009**, *113*, 9718–9727.
18. Kietzke, T.; Neher, D.; Kumke, M.; Montenegro, R.; Landfester, K.; Scherf, U. A Nanoparticle Approach to Control the Phase Separation in Polyfluorene Photovoltaic Devices. *Macromolecules* **2004**, *37*, 4882–4890.
19. Kietzke, T.; Neher, D.; Landfester, K.; Montenegro, R.; Guntner, R.; Scherf, U. Novel Approaches to Polymer Blends Based on Polymer Nanoparticles. *Nat. Mater.* **2003**, *2*, 408–412.
20. Piok, T.; Gamerith, S.; Gadermaier, C.; Plank, H.; Wenzl, F. P.; Patil, S.; Montenegro, R.; Kietzke, T.; Neher, D.; Scherf, U.; *et al*. Organic Light-Emitting Devices Fabricated from Semiconducting Nanospheres. *Adv. Mater.* **2003**, *15*, 800–804.
21. Shimizu, H.; Yamada, M.; Wada, R.; Okabe, M. Preparation and Characterization of Water Self-Dispersible Poly(3-hexylthiophene) Particles. *Polym. J.* **2008**, *40*, 33–36.
22. Huber, J.; Mecking, S. Processing of Polyacetylene from Aqueous Nanoparticle Dispersions. *Angew. Chem., Int. Ed.* **2006**, *45*, 6314–6317.
23. Landfester, K.; Montenegro, R.; Scherf, U.; Guntner, R.; Asawapirom, U.; Patil, S.; Neher, D.; Kietzke, T. Semiconducting Polymer Nanospheres in Aqueous Dispersion Prepared by a Miniemulsion Process. *Adv. Mater.* **2002**, *14*, 651–655.
24. Janietz, S.; Sainova, D. Significant Improvement of the Processability of Ladder-Type Polymers by Using Aqueous Colloidal Dispersions. *Macromol. Rapid Commun.* **2006**, *27*, 943–947.
25. Szymanski, C.; Wu, C. F.; Hooper, J.; Salazar, M. A.; Perdomo, A.; Dukes, A.; McNeill, J. Single Molecule Nanoparticles of the Conjugated Polymer MEH-PPV, Preparation and Characterization by Near-Field Scanning Optical Microscopy. *J. Phys. Chem. B* **2005**, *109*, 8543–8546.
26. Kurokawa, N.; Yoshikawa, H.; Hirota, N.; Hyodo, K.; Masuhara, H. Size-Dependent Spectroscopic Properties and Thermochromic Behavior in Poly(substituted thiophene) Nanoparticles. *ChemPhysChem* **2004**, *5*, 1609–1615.
27. Marini, M.; Pilati, F.; Pourabbas, B. Smooth Surface Polypyrrole-Silica Core−Shell Nanoparticles: Preparation, Characterization and Properties. *Macromol. Chem. Phys.* **2008**, *209*, 1374–1380.
28. Yabu, H.; Higuchi, T.; Ijiro, K.; Shimomura, M. Spontaneous Formation of Polymer Nanoparticles by Good-Solvent Evaporation as a Nonequilibrium Process. *Chaos* **2005**, *15*, 047505.
29. Millstoneaaa, J. E.; Kavulak, D. F. J.; Woo, C. H.; Holcombe, T. W.; Westling, E. J.; Briseno, A. L.; Toney, M. F.; Frechet, J. M. J. Synthesis, Properties, and Electronic Applications of Size-Controlled Poly(3-hexylthiophene) Nanoparticles. *Langmuir* **2010**, *26*, 13056–13061.
30. Ostrowski, D. P.; Lytwak, L. A.; Mejia, M. L.; Stevenson, K. J.; Holliday, B. J.; Vanden Bout, D. A. The Effects of Aggregation on Electronic and Optical Properties of Oligothiophene Particles. *ACS Nano* **2012**, *6*, 5507–5513.
31. Andersen, T. R.; Larsen-Olsen, T. T.; Andreasen, B.; Bottiger, A. P. L.; Carle, J. E.; Helgesen, M.; Bundgaard, E.; Norrman, K.; Andreasen, J. W.; Jorgensen, M.; *et al*. Aqueous Processing of Low-Band-Gap Polymer Solar Cells Using Roll-to-Roll Methods. *ACS Nano* **2011**, *5*, 4188–4196.
32. Hu, Z.; Gesquiere, A. J. Charge Trapping and Storage by Composite P3HT/PC60BM Nanoparticles Investigated by Fluorescence-Voltage/Single Particle Spectroscopy. *J. Am. Chem. Soc.* **2011**, *133*, 20850–20856.
33. Hu, Z.; Tenery, D.; Bonner, M. S.; Gesquiere, A. J. Correlation between Spectroscopic and Morphological Properties of Composite P3HT/PCBM Nanoparticles Studied by Single Particle Spectroscopy. *J. Luminesc.* **2010**, *130*, 771–780.
34. Liu, Z. Y.; Liu, L. J.; Li, H.; Dong, Q. F.; Yao, S. Y.; Kidd, A. B.; Zhang, X. Y.; Li, J. Y.; Tian, W. J. "Green" Polymer Solar Cell Based on Water-Soluble Poly[3-(potassium-6-hexanoate)-thiophene-2,5-diyl] and Aqueous-Dispersible Noncovalent Functionalized Graphene Sheets. *Sol. Energy Mater. Sol. Cells* **2012**, *97*, 28–33.
35. Tenery, D.; Gesquiere, A. J. Interplay between Fluorescence and Morphology in Composite MEH-PPV/PCBM Nanoparticles Studied at the Single Particle Level. *Chem. Phys.* **2009**, *365*, 138–143.
36. Stapleton, A.; Vaughan, B.; Xue, B.; Sesa, E.; Burke, K.; Zhou, X.; Bryant, G.; Werzer, O.; Nelson, A.; Kilcoyne, A. L. D.; *et al*. A Multilayered Approach to Polyfluorene Water-Based Organic Photovoltaics. *Sol. Energy Mater. Sol. Cells* **2012**, *102*, 114–124.
37. Hu, Z.; Gesquiere, A. J. PCBM Concentration Dependent Morphology of P3HT in Composite P3HT/PCBM Nanoparticles. *Chem. Phys. Lett.* **2009**, *476*, 51–55.
38. Larsen-Olsen, T. T.; Andersen, T. R.; Andreasen, B.; Bottiger, A. P. L.; Bundgaard, E.; Norrman, K.; Andreasen, J. W.; Jorgensen, M.; Krebs, F. C. Roll-to-Roll Processed Polymer Tandem Solar Cells Partially Processed from Water. *Sol. Energy Mater. Sol. Cells* **2012**, *97*, 43–49.
39. Burke, K. B.; Stapleton, A. J.; Vaughan, B.; Zhou, X.; Kilcoyne, A. L. D.; Belcher, W. J.; Dastoor, P. C. Scanning Transmission X-ray Microscopy of Polymer Nanoparticles: Probing Morphology on Sub-10 nm Length Scales. *Nanotechnology* **2011**, *22*.
40. Labastide, J. A.; Baghgar, M.; Dujovne, I.; Yang, Y. P.; Dinsmore, A. D.; Sumpter, B. G.; Venkataraman, D.; Barnes, M. D. Polymer Nanoparticle Super Lattices for Organic Photovoltaic Applications. *J. Phys. Chem. Lett.* **2011**, *2*, 3085–3091.
41. Labastide, J. A.; Baghgar, M.; Dujovne, I.; Venkatraman, B. H.; Ramsdell, D. C.; Venkataraman, D.; Barnes, M. D. Time- and Polarization-Resolved Photoluminescence of Individual Semicrystalline Polythiophene (P3HT) Nanoparticles. *J. Phys. Chem. Lett.* **2011**, *2*, 2089–2093.
42. Traub, M. C.; Vogelsang, J.; Plunkett, K. N.; Nuckolls, C.; Barbara, P. F.; Vanden Bout, D. A. Unmasking Bulk Exciton Traps and Interchain Electronic Interactions with Single Conjugated Polymer Aggregates. *ACS Nano* **2012**, *6*, 523–529.
43. Khalil, G. E.; Adawi, A. M.; Robinson, B.; Cadby, A. J.; Tsoi, W. C.; Kim, J. S.; Charas, A.; Morgado, J.; Lidzey, D. G. Spectroscopy and Single-Molecule Emission of a Fluorene−Terthiophene Oligomer. *J. Phys. Chem. B* **2011**, *115*, 12028–12035.
44. Dang, M. T.; Hirsch, L.; Wantz, G. P3HT:PCBM, Best Seller in Polymer Photovoltaic Research. *Adv. Mater.* **2011**, *23*, 3597–3602.
45. Sirringhaus, H.; Brown, P. J.; Friend, R. H.; Nielsen, M. M.; Bechgaard, K.; Langeveld-Voss, B. M. W.; Spiering, A. J. H.; Janssen, R. A. J.; Meijer, E. W.; Herwig, P.; *et al*. Two-Dimensional Charge Transport in Self-Organized, High-Mobility Conjugated Polymers. *Nature* **1999**, *401*, 685–688.
46. Yang, H. C.; Shin, T. J.; Yang, L.; Cho, K.; Ryu, C. Y.; Bao, Z. N. Effect of Mesoscale Crystalline Structure on the Field-Effect Mobility of Regioregular Poly(3-hexylthiophene) in Thin-Film Transistors. *Adv. Funct. Mater.* **2005**, *15*, 671–676.
47. Erb, T.; Zhokhavets, U.; Hoppe, H.; Gobsch, G.; Al-Ibrahim, M.; Ambacher, O. Absorption and Crystallinity of Poly(3-hexylthiophene)/Fullerene Blends in Dependence on Annealing Temperature. *Thin Solid Films* **2006**, *511*, 483–485.
48. Kline, R. J.; McGehee, M. D.; Toney, M. F. Highly Oriented Crystals at the Buried Interface in Polythiophene Thin-Film Transistors. *Nat. Mater.* **2006**, *5*, 222–228.

49. Zhokhavets, U.; Erb, T.; Gobsch, G.; Al-Ibrahim, M.; Ambacher, O. Relation between Absorption and Crystallinity of Poly-(3-hexylthiophene)/Fullerene Films for Plastic Solar Cells. *Chem. Phys. Lett.* **2006**, *418*, 347–350.
50. Jimison, L. H.; Toney, M. F.; McCulloch, I.; Heeney, M.; Salleo, A. Charge-Transport Anisotropy Due to Grain Boundaries in Directionally Crystallized Thin Films of Regioregular Poly(3-Hexylthiophene). *Adv. Mater.* **2009**, *21*, 1568–1572.
51. Pan, L. K.; Sun, Z. Solvent and Temperature-Dependent Conductive Behavior of Poly(3-hexylthiophene). *J. Phys. Chem. Solids* **2009**, *70*, 1113–1116.
52. Salleo, A.; Kline, R. J.; DeLongchamp, D. M.; Chabinyc, M. L. Microstructural Characterization and Charge Transport in Thin Films of Conjugated Polymers. *Adv. Mater.* **2010**, *22*, 3812–3838.
53. Wang, T.; Dunbar, A. D. F.; Staniec, P. A.; Pearson, A. J.; Hopkinson, P. E.; MacDonald, J. E.; Lilliu, S.; Pizzey, C.; Terrill, N. J.; Donald, A. M.; *et al*. The Development of Nanoscale Morphology in Polymer: Fullerene Photovoltaic Blends During Solvent Casting. *Soft Matter* **2010**, *6*, 4128–4134.
54. Xue, L. J.; Gao, X.; Zhao, K.; Liu, J. G.; Yu, X. H.; Han, Y. C. The Formation of Different Structures of Poly(3-hexylthiophene) Film on a Patterned Substrate by Dip Coating from Aged Solution. *Nanotechnology* **2010**, *21*, 145303.
55. Zhao, K.; Xue, L. J.; Liu, J. G.; Gao, X.; Wu, S. P.; Han, Y. C.; Geng, Y. H. A New Method to Improve Poly(3-hexylthiophene) (P3HT) Crystalline Behavior: Decreasing Chains Entanglement to Promote Order-Disorder Transformation in Solution. *Langmuir* **2010**, *26*, 471–477.
56. Brinkmann, M. Structure and Morphology Control in Thin Films of Regioregular Poly(3-hexylthiophene). *J. Polym. Sci,. Part B.* **2011**, *49*, 1218–1233.
57. Roehling, J. D.; Arslan, I.; Moule, A. J. Controlling Microstructure in Poly(3-hexylthiophene) Nanofibers. *J. Mater. Chem.* **2012**, *22*, 2498–2506.
58. Xue, L. J.; Yu, X. H.; Han, Y. C. Different Structures and Crystallinities of Poly(3-hexylthiophene) Films Prepared from Aged Solutions. *Colloid Surf. A* **2011**, *380*, 334–340.
59. Clark, J.; Chang, J. F.; Spano, F. C.; Friend, R. H.; Silva, C. Determining Exciton Bandwidth and Film Microstructure in Polythiophene Films Using Linear Absorption Spectroscopy. *Appl. Phys. Lett.* **2009**, *94*, 163306.
60. Landfester, K. Synthesis of Colloidal Particles in Miniemulsions. *Annu. Rev. Mater. Res.* **2006**, *36*, 231–279.
61. Yamagata, H.; Spano, F. C. Interplay between Intrachain and Interchain Interactions in Semiconducting Polymer Assemblies: The *HJ*-Aggregate Model. *J. Chem. Phys.* **2012**, *136*, 184901.
62. Wang, T.; Pearson, A. J.; Lidzey, D. G.; Jones, R. A. L. Evolution of Structure, Optoelectronic Properties, and Device Performance of Polythiophene: Fullerene Solar Cells During Thermal Annealing. *Adv. Funct. Mater.* **2011**, *21*, 1383–1390.
63. Kim, H.; Ok, S.; Chae, H.; Choe, Y. Performance Characteristics of Polymer Photovoltaic Solar Cells with an Additive-Incorporated Active Layer. *Nanoscale Res. Lett.* **2012**, *7*, 56.
64. Erb, T.; Zhokhavets, U.; Gobsch, G.; Raleva, S.; Stuhn, B.; Schilinsky, P.; Waldauf, C.; Brabec, C. J. Correlation between Structural and Optical Properties of Composite Polymer/Fullerene Films for Organic Solar Cells. *Adv. Funct. Mater.* **2005**, *15*, 1193–1196.
65. Chu, C.-W.; Yang, H.; Hou, W.-J.; Huang, J.; Li, G.; Yang, Y. Control of the Nanoscale Crystallinity and Phase Separation in Polymer Solar Cells. *Appl. Phys. Lett.* **2008**, *92*, 103306.
66. Sandberg, H. G. O.; Frey, G. L.; Shkunov, M. N.; Sirringhaus, H.; Friend, R. H.; Nielsen, M. M.; Kumpf, C. Ultrathin Regioregular Poly(3-hexylthiophene) Field-Effect Transistors. *Langmuir* **2002**, *18*, 10176–10182.
67. Spano, F. C. The Spectral Signatures of Frenkel Polarons in *H*- and *J*-Aggregates. *Acc. Chem. Res.* **2010**, *43*, 429–439.
68. Aiyar, A. R.; Hong, J. I.; Nambiar, R.; Collardaaa, D. M.; Reichmanis, E. Tunable Crystallinity in Regioregular Poly-(3-hexylthiophene) Thin Films and Its Impact on Field Effect Mobility. *Adv. Funct. Mater* **2011**, *21*, 2652–2659.
69. Machui, F.; Langner, S.; Zhu, X. D.; Abbott, S.; Brabec, C. J. Determination of the P3HT:PCBM Solubility Parameters *via* a Binary Solvent Gradient Method: Impact of Solubility on the Photovoltaic Performance. *Sol. Energy Mater. Sol. Cells* **2012**, *100*, 138–146.